ARTICLE NO. 79-0609bR

Influence of Propeller Design Parameters on Far-Field Harmonic Noise in Forward Flight

Donald B. Hanson*
Hamilton Standard Div., United Technologies Corporation, Windsor Locks, Conn.

A theory for harmonic noise radiation is studied for general guidance to the designer and is applied to some propeller noise problems of current interest. Only the linear sources are studied in detail. The frequency domain results clarify the role of acoustic noncompactness (noise cancellation due to finite chord and span effects). Nondimensional parameters arising from the analysis give design guidance by showing the potential for noise reduction due to changes in airfoil section and blade sweep, twist, and taper as functions of operating conditions. Conventional propellers are shown to be relatively insensitive to variations in blade design. However, advanced turbopropellers (prop fans) currently under development are decidedly noncompact because of their high solidity and speed. Examples of chordwise and spanwise cancellation are given illustrating substantial benefits of sweep.

Nomenclature

b	= airfoil chord
B	= number of blades
$B_D \equiv b/D$	= chord-to-diameter ratio
c_0	= ambient speed of sound
C_L	= section lift coefficient
D	= propeller diameter
FA	= face alignment or offset, see Fig. 3
H	= normalized thickness distribution Fig. 2
J_n	= Bessel function
k_x, k_y	= wave numbers given by Eqs. (5) and (6)
m	= harmonic of blade passing frequency
MCA	= midchord alignment or sweep, see Fig. 3
M_r	= $\sqrt{M_x^2 + z^2 M_T^2}$ section relative Mach number
M_T	= $\Omega r_T / c_0$ = tip rotational Mach number
M_x	= V/c_0 = flight Mach number
r_T	= propeller tip radius = $D/2$
t	= observer time
t_b	= ratio of section maximum thickness to chord
V	= flight speed
X	= normalized chordwise coordinate
y	= observer distance from propeller axis
z	= normalized radial coordinate (= 1 at tip)
θ	= radiation angle from propeller axis to observer
ϕ_o, ϕ_s	= phase lag due to offset and sweep, Eqs. (7) and (8)
Ψ_V, Ψ_L	= transforms of thickness and lift source terms, Eqs. (3) and (4)
Ω	= 2π times shaft rotation frequency
Ω_D	= $\Omega/(1 - M_x \cos\theta)$

Introduction

GIVEN the task of designing a propeller for a particular application, the engineer has some freedom to choose design parameters for reduced noise. The traditional approaches of decreasing diameter, reducing tip speed, or increasing the number of blades are all effective but have important impact on aerodynamic efficiency, weight, and cost.

In this paper, however, the emphasis will be on noncompactness as related to parameters which are less understood, namely airfoil section shape and sweep, twist, and chord distributions. It will also be shown how the sensitivity to these parameters is influenced by operating conditions.

To focus the discussion, four noise situations of current interest have been selected for study and are given in Table 1. The general aviation (GA) propeller typically has two blades and operates at high tip speeds. The condition shown in the table is for the flyover required for certification for a small general aviation aircraft with a single-piston engine.

The large conventional (LC) aircraft is a multiengine turboprop operating at lower propeller speed by use of a gearbox. The conditions shown are for takeoff. For the prop fan (PF) category (Fig. 1), a multiengine aircraft is shown both in takeoff and cruise. In takeoff, it is similar to the LC aircraft. However, in cruise, the high forward speed results in

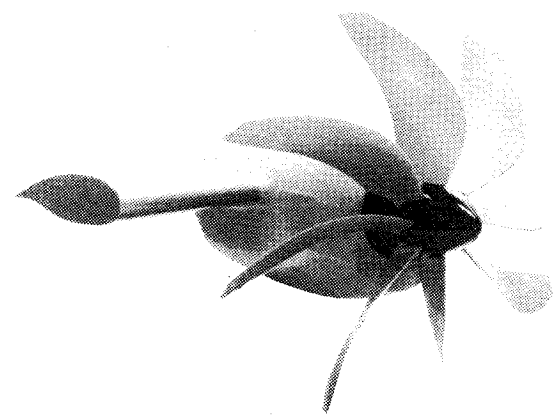

Fig. 1 Prop fan propulsor.

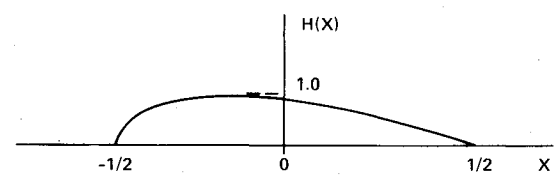

Fig. 2 Normalized thickness distribution.

Presented as part of Paper 79-0609 at the AIAA 5th Aeroacoustics Conference, Seattle, Wash., March 12-14, 1979; submitted May 23, 1979; revision received Dec. 27, 1979.

Index categories: Aeroacoustics; Noise; Propeller and Rotor Systems.

*Principal Research Engineer, Design Department, Aircraft Systems Division.

Table 1 Propeller noise categories chosen for discussion

	GA propeller (flyover)	LC propeller (takeoff)	Prop fan (Takeoff)	Prop fan (Cruise)
No. of blades	2	4	8	8
Flight Mach no. M_x	0.276	0.212	0.228	0.8
Tip rotational Mach no. M_T	0.857	0.648	0.719	0.822
Tip helical Mach no. M_r	0.900	0.682	0.754	1.147
Harmonic range mB of primary concern	10-20	4-12	8-12	8-12

supersonic tip relative speeds. The major concern here is the cabin noise in the near field where the theory derived above is not strictly valid. However, the good agreement shown in Fig. 8 of Ref. 1 for 0.8 diameter tip clearance justifies use of the theory to study trends and sensitivity to changes in design parameters.

Theoretical Background

In Ref. 1 the following formulas were derived for the complex Fourier harmonics of thickness noise P_{VM} and loading noise P_{LM}.

$$\left\{\begin{matrix} P_{Vm} \\ P_{Lm} \end{matrix}\right\} = \frac{\rho_0 c_0^2 B \sin\theta \exp\left[imB\left(\frac{\Omega_D r}{c_0} - \frac{\pi}{2}\right)\right]}{8\pi \frac{y}{D}(1-M_x\cos\theta)} \int M_r^2 e^{i(\phi_o+\phi_s)} \times J_{mB}\left(\frac{mBzM_T\sin\theta}{1-M_x\cos\theta}\right)\left\{\begin{matrix} -k_x^2 t_b \Psi_V(k_x) \\ ik_y (C_L/2)\Psi_L(k_x) \end{matrix}\right\} dz \quad (1)$$

The convention for these harmonics is such that the acoustic pressure waveforms can be computed from either of the two equivalent expressions

$$p(t) = \sum_{m=-\infty}^{\infty} P_{mB} e^{-imB\Omega_D t} \quad (2a)$$

$$p(t) = 2 \times \text{Real part} \sum_{m=1}^{\infty} P_{mB} e^{-imB\Omega_D t} \quad (2b)$$

Ψ_V and Ψ_L are Fourier transforms of the chordwise thickness and loading distributions given by

$$\Psi_V(k_x) = \int_{-1/2}^{1/2} H(x) e^{ik_x X} dX \quad (3)$$

$$\Psi_L(k_x) = \int_{-1/2}^{1/2} f_L(X) e^{ik_x X} dX \quad (4)$$

where $H(X)$ is the normalized thickness distribution shown in Fig. 2 and $f_L(X)$ is a similar curve giving the shape of the chordwise loading distribution. $f_L(X)$ is normalized so that its area $\Psi_L(0) = \int f_L(X) dX = 1.0$. k_x and k_y are wave numbers defined by

$$k_x = \frac{2mBB_D M_T}{M_r(1-M_x\cos\theta)} \quad (5)$$

and

$$k_y = \frac{2mBB_D}{zM_r}\left(\frac{M_r^2\cos\theta - M_x}{1-M_x\cos\theta}\right) \quad (6)$$

which will be shown shortly to be measures of noncompactness.

Finally, ϕ_s and ϕ_o are phase shifts due to sweep and offset and are given by

$$\phi_s = \frac{2mBM_T}{M_r(1-M_x\cos\theta)} \frac{\text{MCA}}{D} \quad (7)$$

and

$$\phi_o = \frac{2mB}{zM_r}\left(\frac{M_r^2\cos\theta - M_x}{1-M_x\cos\theta}\right) \frac{\text{FA}}{D} \quad (8)$$

MCA and FA are the midchord alignment (or sweep) and face alignment (or offset) defined with the three Mach numbers M_x, M_T, and M_r in Fig. 3.

The radiation angle θ is measured from the flight direction at the location of the aircraft when it emitted the sound. The Appendix shows how θ is related to the angle θ_1 measured from the current aircraft location.

Influence of Design Parameters

Because noise sensitivities vary with directivity or radiation angle θ, the first section below will address directivity patterns for the four noise categories. This will allow the investigation of sensitivities at the peak noise locations. This is followed by sections on chordwise distribution effects and spanwise distribution effects.

Directivity Effects

For a representative radius on a straight blade, the directivity pattern at a constant altitude or sideline distance y can be obtained from Eqs. (1, 5, and 6). For thickness, the directivity index (DI) is

$$(\text{DI})_V = \frac{\sin\theta}{(1-M_x\cos\theta)^3} J_{mB}\left(\frac{mBzM_T\sin\theta}{1-M_x\cos\theta}\right)\Psi_V(k_x) \quad (9)$$

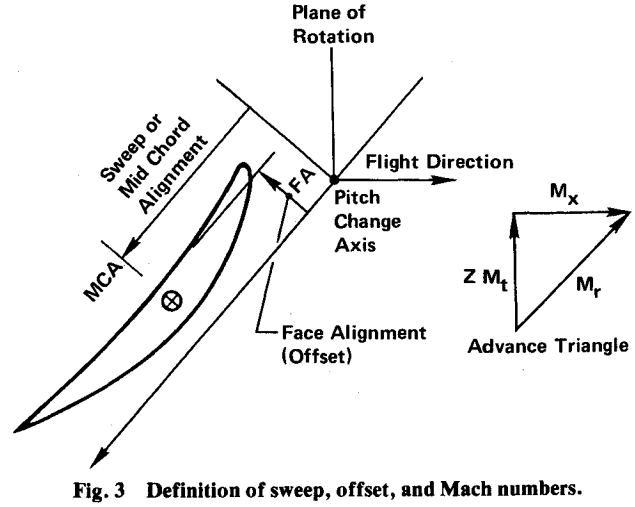

Fig. 3 Definition of sweep, offset, and Mach numbers.

For loading,

$$(\mathrm{DI})_L = \frac{\sin\theta}{(1-M_x\cos\theta)^2}\,(M_r^2\cos\theta - M_x)\,J_{mB}\left(\frac{mBzM_T\sin\theta}{1-M_x\cos\theta}\right)\Psi_L(k_x) \qquad (10)$$

Plots of these directivity patterns for the four noise categories are given in Figs. 4-6. For the general aviation propeller, noise is dominated by harmonics in the range of $mB = 10\text{-}20$. Figure 4 shows that the peak radiation angles are $\theta = 70\text{-}90$ deg. The large conventional propeller and the prop fan at takeoff have the directivity peaks in the same range. However, the prop fan in cruise, shown at the bottom of Fig. 6, radiates much further forward because of the strong Doppler effect at 0.8 flight Mach number. The thickness noise peaks at $\theta \approx 30$ deg and the loading noise has two strong peaks at $\theta \approx 25$ and 60 deg. (Note that the front loading peak is not dominant for all source radii.)

Chordwise Distribution Effects (Airfoil Shape)

Thickness Noise

In the radiation integral for thickness noise [top half of Eq. (1)], the factors influenced by airfoil section geometry at a given radius are

$$t_b B_D^2 \Psi_V(k_x) = \text{chordwise thickness geometry term} \qquad (11)$$

where t_b is the section thickness-to-chord ratio and B_D is the section chord-to-diameter ratio. Since the product $t_b B_D^2$ is proportional to the airfoil cross-sectional area, the noise from a radial strip dz is proportional to $t_b B_D^2 dz$, i.e., to the volume displaced by the strip. For structural reasons, changes in chord are often made at constant t_b; in these cases, thickness noise is proportional to B_D^2.

The factor $\Psi_V(k_x)$ is the Fourier transform of the chordwise thickness distribution and accounts for chordwise noncompactness as a function of the wave number $k_x = 2\,mBB_DM_T/M_r\,(1-M_x\cos\theta)$. Figure 7 was prepared to help find the numerical values of k_x that should be considered. The lower portion of the figure shows that, for the first three noise categories of Table 1, k_x is relatively insensitive to radiation angle and section rotational Mach number zM_T. The points indicated by ⊙ in Fig. 7 correspond to the peak radiation angles found from Figs. 4-6 and suggest using $k_x = 2\,mBB_D/z$ for the first three noise categories ($M_x \approx 0.25$). The upper part of Fig. 7 applies to the prop fan cruise category and indicates a greater dependence upon θ and larger values of k_x ($k_x \approx 4mBB_D/z$). The magnitude of Ψ_V is plotted in Fig. 8 for

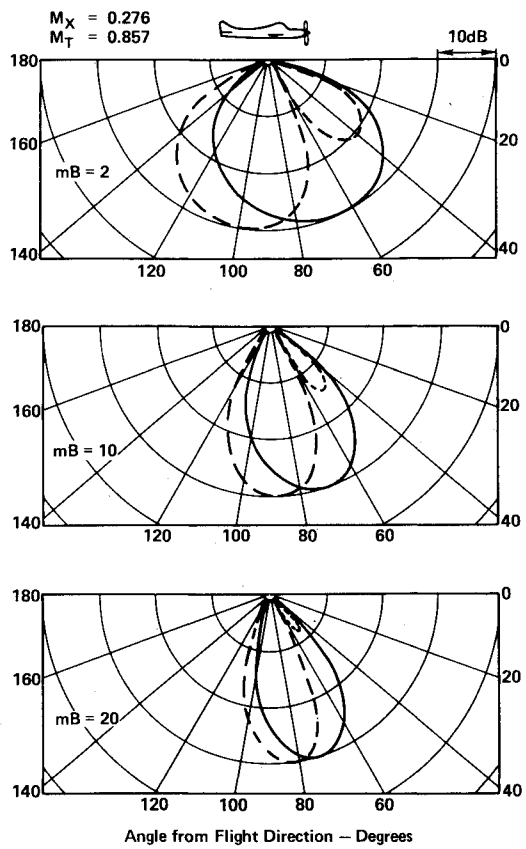

Fig. 4 Directivity patterns for thickness (—) and loading (---) noise from blade element at radius $r_0 = 0.8\,r_T$ (Mach numbers typical for general aviation propeller flyover).

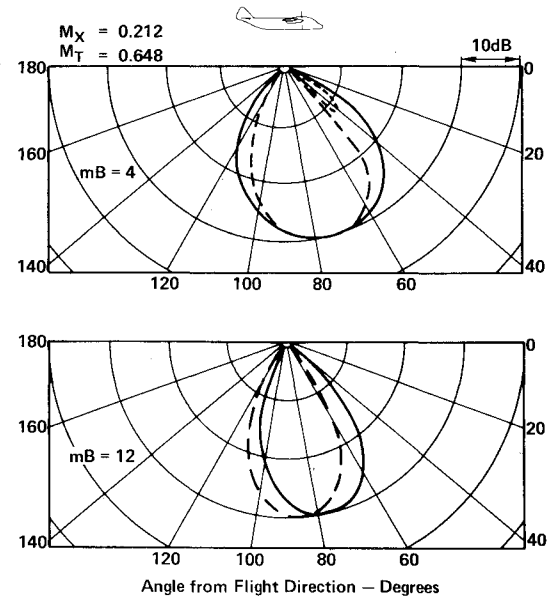

Fig. 5 Directivity patterns for thickness (—) and loading (---) noise from blade element at radius $r_0 = 0.8\,r_T$ (Mach numbers typical for large conventional propeller takeoff).

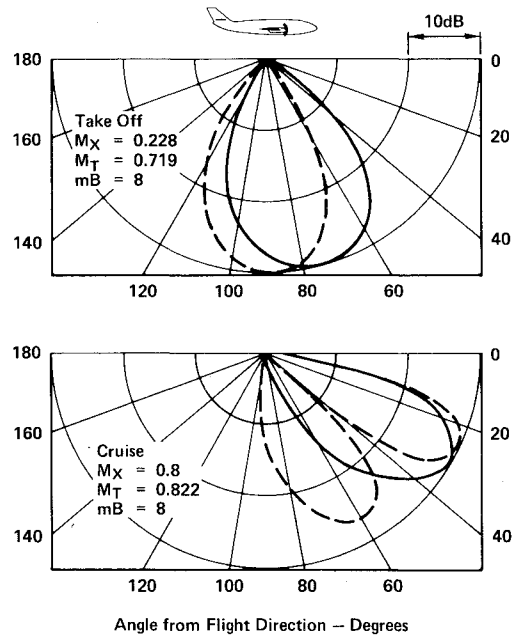

Fig. 6 Directivity patterns for thickness (—) and loading (---) noise from blade element $r_0 = 0.8\,r_T$ (Mach numbers typical for prop fans at takeoff and cruise).

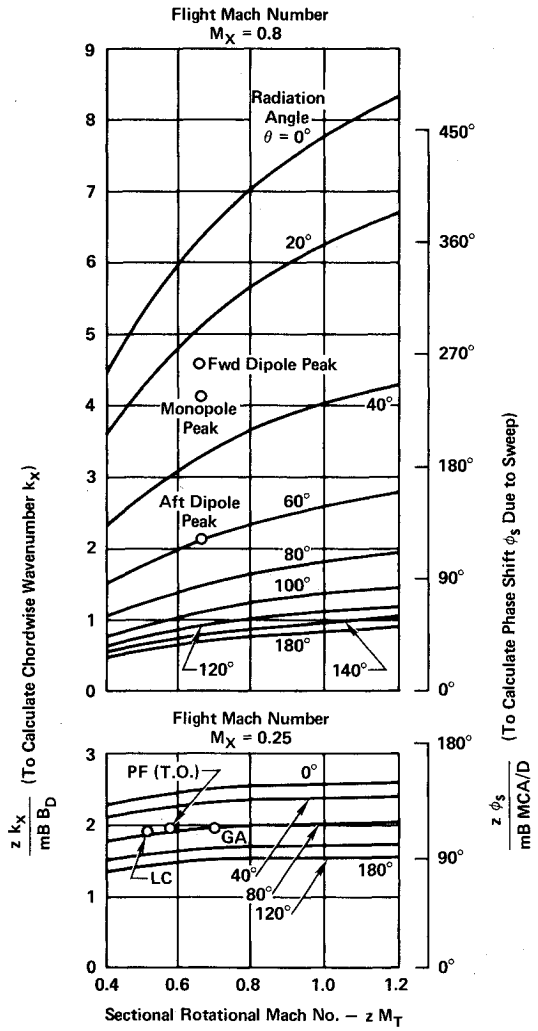

Fig. 7 Graphs to determine chordwise wave number k_x or phase shifts ϕ_s due to sweep as functions of blade geometry and operating Mach numbers.

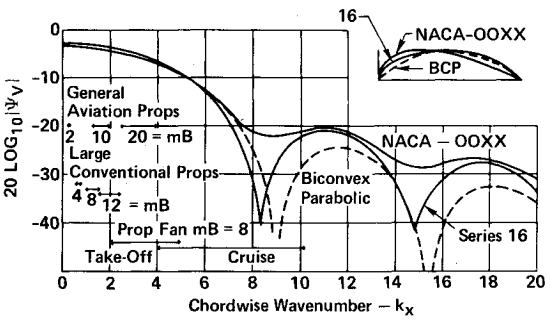

Fig. 8 Reduction of thickness noise from blade element due to chordwise noncompactness.

the three airfoil types. The ranges of k_x for the four noise categories, indicated by the double-headed arrows, were established by choosing $B_D = 0.06$ and $z = 0.6$-1.0 for GA and LC propellers and $B_D = 0.1$-0.2 and $z = 0.6$-1.0 for prop fans.

Figure 8 illustrates some important points relevant to the effect of airfoil section shape on thickness noise: For the first three noise categories, noncompactness effects are relatively small and variations in section shape have no influence. For the prop fan cruise condition, there is somewhat greater sensitivity with the Series 16 thickness distribution looking good. Figure 8 shows that the prop fan in cruise benefits greatly from chordwise noncompactness; calculations with a compact source theory such as that of Arnoldi[2] would be 10-

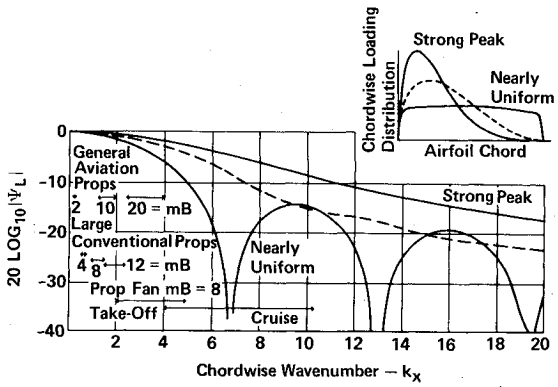

Fig. 9 Reduction of loading noise from blade element due to chordwise noncompactness.

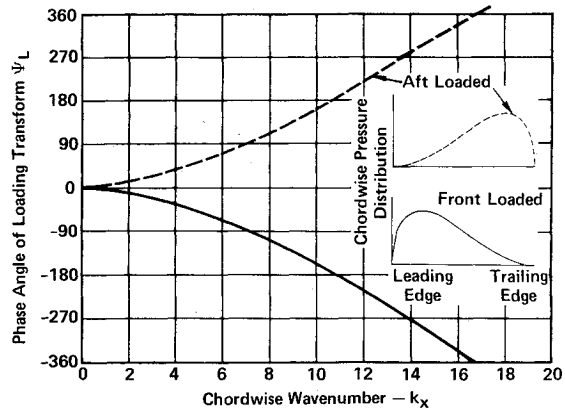

Fig. 10 Effect of chordwise shift in loading distribution on phase lag of signal from blade element.

20 dB pessimistic at blade passing frequency and worse at the higher harmonics.

Loading Noise

In the radiation integral for loading noise [bottom half of Eq. (1)], the factors influenced by airfoil section geometry are

$$C_L B_D \Psi_L(k_x) = \text{chordwise loading geometry term} \qquad (12)$$

where C_L is the section lift coefficient and B_D is the chord-to-diameter ratio. Thus, loading noise is proportional to $C_L B_D$, i.e., to section lift. The factor $\Psi_L(k_x)$ is the Fourier transform of the chordwise loading distribution, which is controlled by angle of attack, camber, and Mach number. Ψ_L acts according to the same principles described above for Ψ_V as shown in Fig. 9. The difference is that, in practice, there will be much greater variations in chordwise loading distributions than in thickness distributions.

Figure 9 shows that "peak" distributions should be avoided in order to benefit from chordwise noncompactness, particularly for the prop fan cruise conditions. A related point is that accurate noise predictions for the prop fan require accurate estimates of chordwise loading distributions.

Chordwise distribution also affects the phase of Ψ_L as illustrated in Fig. 10. Shifting the load toward the trailing edge causes a phase lag, as would be expected. In principle, this could be used to promote phase cancellation between signals from different radii on the blade. This would be difficult in practice, however, because the required peak loadings would increase the amplitudes of the signals to be cancelled.

Spanwise Distribution Effects

In Eq. (1) the radial integrals for thickness and loading noise were found to be

$$\int_0^1 J_{mB}(\cdot)e^{i(\phi_o+\phi_s)}t_bB_D^2\Psi_V(k_x)\,dz = \text{radial thickness integral} \tag{13}$$

and

$$\int_0^1 \frac{M_r}{z}(M_r^2\cos\theta - M_x)J_{mB}(\cdot)e^{i(\phi_o+\phi_s)}C_LB_D\Psi_L(k_x)\,dz = \text{radial loading integral} \tag{14}$$

Ψ_V and Ψ_L contain all the chordwise distribution information and were discussed in detail above. For the discussion to follow, it will be assumed that Ψ_V and Ψ_L have zero phase angle as would be the case for chordwise distributions with fore and aft symmetry (e.g., uniform loading). Also, J_{mB} and $(Mr/z)(M_r^2\cos\theta - M_x)$ do not include any blade geometry and will not be discussed further.

The remaining items for discussion are then $e^{i(\phi_o+\phi_s)}t_bB_D^2$ for thickness noise and $e^{i(\phi_o+\phi_s)}C_LB_D$ for loading noise. For straight blades ($\phi_o=\phi_s=0$), the signals from each radial station on the blade are exactly in phase except for possible sign changes which occur in the Ψ's around $k_x=7$-9 and in $M_r^2\cos\theta - M_x$. Effective radius calculation techniques, which eliminate the radial integrations in Eqs. (13) and (14), are valid only for $\phi_o=\phi_s=0$. For straight blades, the only guidance for thickness noise is to reduce $t_bB_D^2$ as much as possible within structural and aerodynamic constraints. For loading noise, there is some flexibility to adjust the radial load distribution C_L by changing blade twist; an example is given later. Finally, for swept or offset blades (ϕ_s or $\phi_o \neq 0$), phase variations along the span can cause significant destructive interference. This is discussed in the next section.

Sweep

Sweeping a blade has two beneficial effects. The first is the relief of transonic compressibility via the same principles used for swept wing design. This acts to reduce the strength of the quadrupole sources as they are primarily transonic flow phenomena. The second effect is to "dephase" noise signals radiating from different portions of the blade.

This is illustrated in Fig. 11 where one harmonic of the noise radiated at angle θ is considered. By performing the chordwise surface integrals first via Eqs. (3) and (4), it is legitimate to treat the noise as coming from many strips on the blade. Since only one harmonic at a time is considered, the noise from strip number j is described completely by its amplitude A_j and its phase ϕ_j in the complex notation $A_je^{i(-mB\Omega t+\phi_j)}$. The total noise is the sum of the strip contributions:

$$A_Re^{i\phi_R} = \sum_{j=1}^{N} A_je^{i\phi_j} \tag{15}$$

where the common factor $e^{-imB\Omega t}$ has been cancelled from both sides. This complex addition is easily visualized as the head-to-tail vector addition, also shown in Fig. 12. By sweeping the blade sections back, the phase angles of their signals lag and the vector addition plot tends to close on itself, representing the phase interference effect. The amount of phase lag obtained for a given amount of sweep (or midchord alignment, MCA) was given by Eq. (7).

The dependence of this sensitivity to sweep upon operating condition and radiation angle can be evaluated using the right-hand ordinate in Fig. 7. As was the case with chordwise interference effects, interference due to sweep is much more

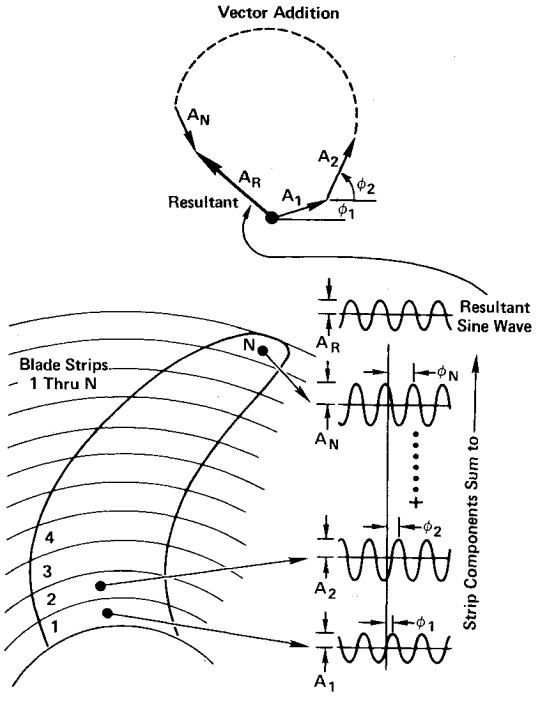

Fig. 11 Acoustician's concept of benefit of sweep: resultant signal is the sum of elemental contributions at all radii (sweep causes signals from the tip to lag in phase and interfere with signals from other radii).

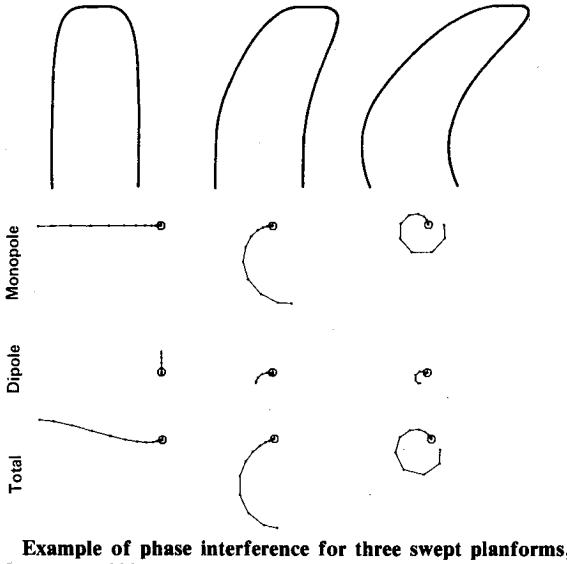

Fig. 12 Example of phase interference for three swept planforms, $M_x=0.8$, $M_T=0.822$, $mB=8$ (vector segments between two dots corresponds to 5% of blade radius, peak radiation angle = 30 deg).

effective at high flight Mach numbers. This is because the phase lag is proportional to the ratio of MCA to the sound wavelength, specifically the Doppler wavelength, which is small at the peak radiation directions.

Examples of phase interference calculations are shown in Fig. 12 for three planforms which are identical except for sweep. The flight condition corresponds to the prop fan cruise case in Table 1 and the spanwise thickness and loading distributions are given by Figs. 6 and 7 of Ref. 1. Chordwise distributions are parabolic to eliminate any phase variations due to airfoil section effects. The left-hand plot, for the straight planform, shows that the phases of the monopole and dipole signals are constant along the span and that they are 90 deg out of phase with each other as required by the appearance of the i multiplying k_y in Eq. (1). Figure 12 shows that adequate sweep can be highly effective at this operating

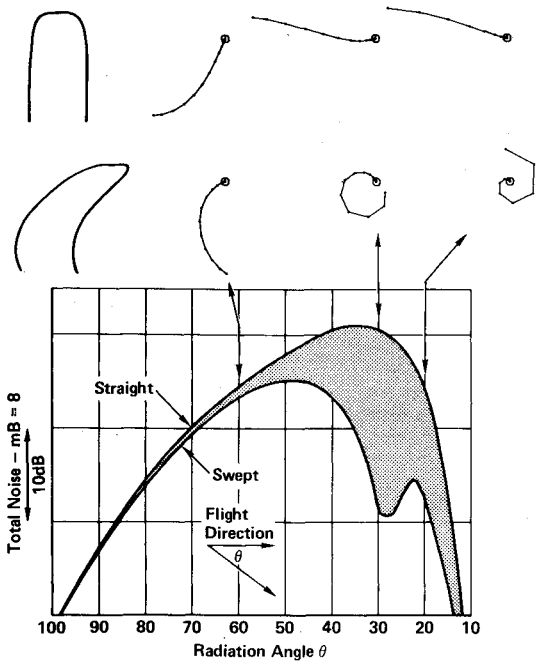

Fig. 13 Directivity dependence of phase interference due to sweep at prop fan cruise condition.

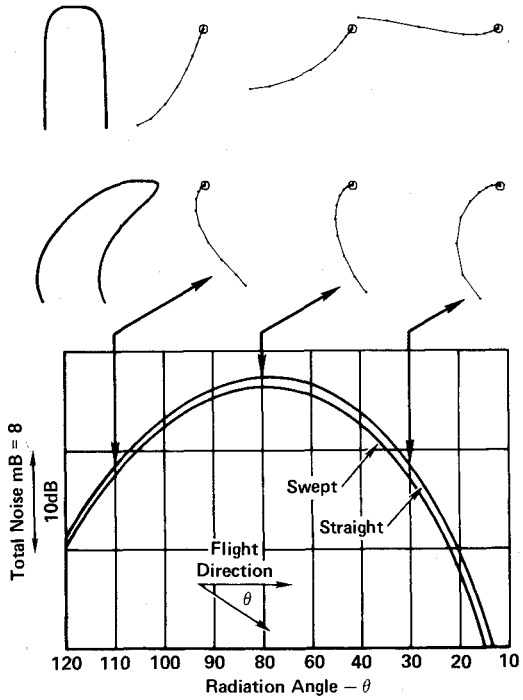

Fig. 14 Directivity dependence of phase interference due to sweep at prop fan takeoff condition $mB = 8$.

condition and radiation angle. The effectiveness does, however, depend upon radiation angle. As shown in Fig. 13, the cancellation is not equally good everywhere but a great deal of energy can be removed from the directivity pattern. At lower flight speed, phase cancellation due to sweep becomes less effective as shown in Fig. 14 for the prop fan takeoff condition. For GA and LC propellers, where the higher harmonics are dominant, sweep can be effective even at low flight speed because of the mB dependence in Eq. (7). For all propeller categories, sweep should be effective in reducing the amplitude of quadrupole sources even if the phase cancellation is ineffective.

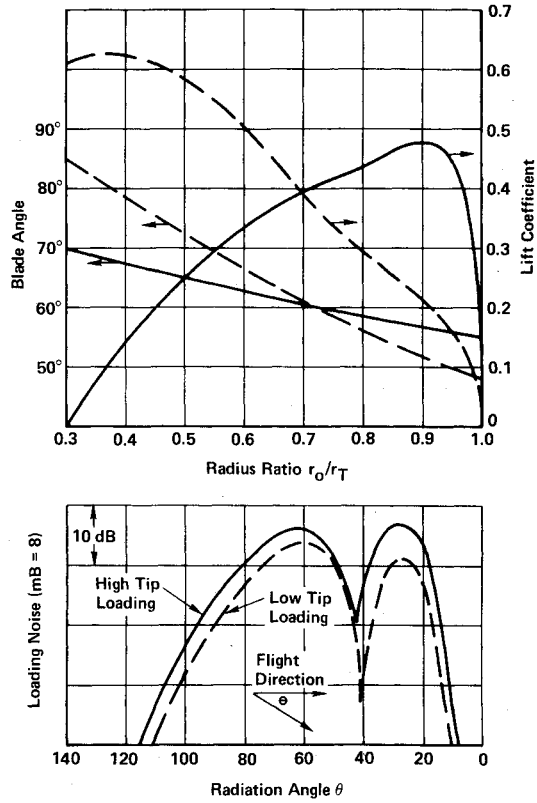

Fig. 15 Effect on loading distribution and noise of extreme changes in blade twist at constant power: prop fan cruise conditions, power coefficient = 1.7 (planform at top left in Fig. 14).

Offset

Offset or face alignment (FA) is the bending of the blade in a direction perpendicular to the chord. This can occur due to dynamic effects or it may be purposely built into a blade. The phase variation due to offset is given by Eq. (8).

Offset is not an effective phase cancellation tool because only small values of FA can be achieved in practice and because the sign of ϕ_o is different on different lobes of the dipole directivity pattern (i.e., for different signs of $M_r^2\cos\theta - M_x$).

Twist

Small changes in twist can cause large changes in radial load distribution because the range in angle of attack from zero lift to stall is only about 10 deg. An extreme example is shown in Fig. 15 to illustrate the principle even though it may not be reasonable for aerodynamic performance. An eight-blade propeller with the planform shown at the upper left in Fig. 14 is operating at the prop fan cruise condition of Table 1. The blade angle (twist) distributions shown in Fig. 15 result in the same absorbed horsepower but very different distributions of lift coefficient. The associated differences in loading noise (at the bottom in Fig. 15) show the acoustic benefits of moving the load away from the high-speed portion of the blade. The effect is equivalent to that of reducing diameter at constant rpm: a noise reduction at some sacrifice in aerodynamic efficiency.

Conclusions

A new theoretical analysis has been explored to determine the influence of propeller design parameters on noise. Effects of noncompactness and forward flight are included for the thickness and lift sources. Because of the far-field, frequency domain formulation, the analytical results are simple and instructive. Highlights of the study are:

1) Noise from a blade element at a single radius can be expressed as products of amplitude and chordwise

distribution factors: $t_b B_D^2 \Psi_V$ for thickness and $C_L B_D \Psi_L$ for loading. The amplitude factors $t_b B_D^2$ and $C_L B_D$ are proportional to section cross-sectional area and section lift, respectively. The factors Ψ_V and Ψ_L are Fourier transforms of the chordwise thickness and loading distributions which account for chordwise noncompactness. It was shown that this effect does reduce thickness noise but that, in the range of practical variations, airfoil section shape does not make a great deal of difference. Chordwise loading distributions, controlled by camber, angle of attack, and Mach number, have much greter variability and thus must be treated with more care. Uniform loading distributions are shown to be much quieter than "peaky" ones, particularly at high frequency.

2) The spanwise distribution effects are sweep, offset, and twist. The effects of sweep are to reduce quadrupole source strength by relief of transonic compressibility and to cause destructive interference between signals from different radii on the blade. A graphical technique was presented for visualization of the interference effect.

A simple formula was found for the phase lag due to sweep, MCA, at a given radius:

$$\phi_s = \frac{2mBM_T}{M_r(1-M_x\cos\theta)} \frac{\text{MCA}}{D}$$

This shows that the effectiveness of sweep increases with harmonic order mB and with flight Mach number M_x.

3) Offset, or bending of the blade perpendicular to the chord, is also accounted for as a phase variation effect. However, this is less effective because of physical constraints.

4) Twist of the blade controls spanwise distribution of loading amplitude. Moving the load inboard to a radius where it radiates less efficiently can reduce noise. However, the penalty in aerodynamic efficiencies must be considered.

5) The sensitivity of noise to variations in the above parameters increases with harmonic order because it is related to the ratio of blade dimension to acoustic wavelength. The sensitivity also increases strongly with flight Mach number because the relevant wavelength is the Doppler wavelength. This puts the prop fan into a unique position because, in cruise at 0.8 Mach number, the Doppler factor is about 3 at the peak radiation angle. Thus, the noise responds significantly to practical geometry changes even at the lowest frequency of interest, blade passing frequency.

Appendix: Relations between Visual and Retarded Reference Systems

Preceding theories[2,3] for forward-flight propeller harmonic noise were derived for a moving fluid with the aircraft and observer fixed in the reference system. In this paper, the observer and fluid are fixed with respect to the reference system and the aircraft flies past at speed V. Although this is truly a transient formulation, it is equivalent to preceding results because the far-field approximation causes the signal to appear periodic (at the Doppler frequency). This Appendix shows how the results from the two formulations are related. The fixed observer system was chosen because the Doppler factor $1/(1-M_x\cos\theta)$ appears explicitly in the results.

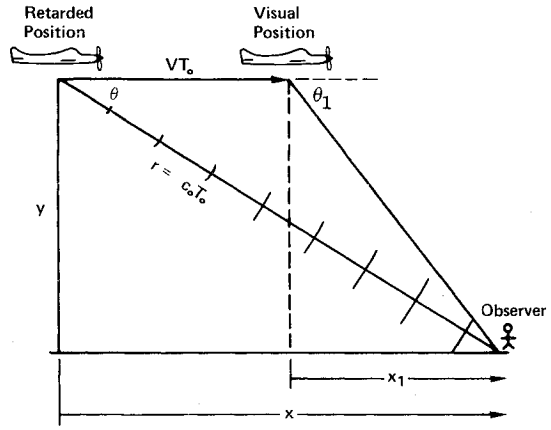

Fig. A1 Sketch for visual and retarded location relations.

Figure A1 shows the geometry. The sound is radiated from the retarded aircraft location and travels a distance $r=c_0T_0$ to the observer position in time T_0. In the same time, the aircraft travels a distance VT_0. Whereas this paper uses observer locations x,y,θ, and $r=\sqrt{x^2+y^2}$, the moving observer theories use x_1,y,θ_1, and a coordinate S_0:

$$S_0=\sqrt{x_1^2+\beta^2y^2} \tag{A1}$$

where $\beta^2=1-M_x^2$. Simple trigonometry leads to the following relationships which can be used to switch references.

$$S_0=r(1-M_x\cos\theta) \tag{A2}$$

$$x=[x_1+M_x\sqrt{x_1^2+\beta^2y^2}]/\beta^2 \tag{A3}$$

$$x_1=x-M_x\sqrt{x^2+y^2} \tag{A4}$$

$$\theta=\arctan(y/x), \text{ radiation angle} \tag{A5}$$

$$\theta_1=\arctan(y/x_1), \text{ visual angle} \tag{A6}$$

For example, in Ref. 3 the Bessel function argument is $mB\Omega yr_0/c_0S_0$. The above formulas can be used to show that

$$J_{mB}\left(\frac{mB\Omega yr_0}{c_0S_0}\right)=J_{mB}\left(\frac{mBzM_T\sin\theta}{1-M_x\cos\theta}\right) \tag{A7}$$

References

[1] Hanson, D. B., "Helicoidal Surface Theory for Harmonic Noise of Propellers in the Far Field," *AIAA Journal*, Vol. 18, Oct. 1980, pp. 1213-1220.

[2] Arnoldi, R. A., "Propeller Noise Caused by Blade Thickness," United Aircraft Research Dept., East Hartford, Conn., Rept. R-0896-1, 1956.

[3] Garrick, I. E., and Watkins, C. E., "A Theoretical Study of the Effects of Forward Speed in the Free-Space Sound-Pressure Field Around Propellers," NACA Rept. 1198, 1954.